Nanoscale

Cite this: *Nanoscale*, 2012, **4**, 1557

www.rsc.org/nanoscale

COMMUNICATION

Nondestructive volumetric 3-D chemical mapping of nickel-sulfur compounds at the nanoscale

William M. Harris,[a] George J. Nelson,[a] Andrew M. Kiss,[a] John R. Izzo, Jr.,[a] Yong Liu,[b] Meilin Liu,[b] Steve Wang,[c] Yong S. Chu[d] and Wilson K. S. Chiu*[a]

Received 9th November 2011, Accepted 6th January 2012
DOI: 10.1039/c2nr11690a

Nano-structures of nickel (Ni) and nickel subsulfide (Ni_3S_2) materials were studied and mapped in 3D with high-resolution x-ray nanotomography combined with full field XANES spectroscopy. This method for characterizing these phases in complex microstructures is an important new analytical imaging technique, applicable to a wide range of nanoscale and mesoscale electrochemical systems.

Nanostructured functional materials found in a number of modern devices frequently consist of multiple distinct phases arranged in a complex, highly irregular structure. Such phases may include either those intentionally incorporated into the structure, or additional poisoning phases resulting from impurities present in the system during fabrication or operation. Examples of the former include different types of batteries and solar cells. Nano-scale nickel sulfide compounds have recently received attention as an attractive cathode material in lithium ion batteries due to their high theoretical capacity.[1–4] Sodium batteries have made use of nickel sulfide phases as well, due to low cost, long life cycle, and good performance.[5,6] Solar cells have also seen recent advances due to the development of new fabrication techniques involving nano-scale structures replacing traditional, expensive platinum counter electrodes.[7]

The presence of undesirable contaminants in a system, even in concentrations in the ppm level, can often result in the formation of solid phases within the microstructure, creating a poisoning effect. In particular, many chemical and electrochemical energy conversion devices suffer from sulfur poisoning of catalyst materials by the formation of solid sulfur-containing phases, leading to a decrease in the number of active sites. Such poisoning may occur for contaminant concentrations between 1 ppm and 10 ppm.[8–12] Due to its significant effect on performance, this poisoning phenomenon has received considerable attention in a number of fields, including the reformation of tar resulting from biomass gasification,[13,14] automobile storage-reduction catalytic converters for the reformation of NO_x,[15,16] treatment of unburned exhaust methane from natural gas power systems,[16,17] steam reformation of liquid hydrocarbons,[18,19] and electrochemical oxidation of readily available fuels in solid oxide fuel cells (SOFCs). High operating temperature and fuel flexibility of SOFCs allow for cost-effective and energy efficient conversion to electricity of hydrocarbon fuels such as natural gas, anaerobic digesters, or syngas, a mixture of H_2 and CO produced from the gasification of fossil fuel or biomass feedstocks. However, the presence of sulfur containing compounds in these fuels may occur due to propagation from the feedstock material or by its introduction as an odorant. Although some work has been done to enhance the tolerance of SOFC anode materials to sulfur poisoning,[20–23] sulfur is still a widely recognized poisoning agent for the commonly used Ni-based anodes.

Past studies have reported SOFC poisoning through a number of mechanisms, including the adsorption of elemental sulfur on the nickel surface and possible formation of nickel sulfide phases,[3,8–10,24] which may occur on different time and length scales. Adsorption of sulfur species on the nickel surface could cause a drop in cell performance due to a reduction in the number of active sites available for electrochemical oxidation of fuels. Such an effect would be fast, leaving a very thin layer of sulfur or sulfur species on the electrode surface.[3] The formation of nickel sulfide phases within the microstructure would be a slower process, taking minutes or longer, and has been shown to be dependent on fuel cell thermal and power cycling conditions.[10] Such phases could form with length scales on the order of microns, akin to a typical SOFC anode.[3,10,25] New phases of this size could have significant effects on the electrode microstructure and performance by blocking gas diffusion pathways and severing electronic and ionic percolation networks. However, at this point, little is known about the detailed 3D formation of these phases, including their size, location, and propensity within unique microstructures.

Recent advances in optics and instrumentation have made x-ray microscopy an effective technique for the investigation of such poisoning effects at the nano-scale.[25–30] Specifically, full-field transmission x-ray microscopy (TXM) provides rapid three-dimensional imaging of complex microstructural materials at better than 20 nm

[a]*Department of Mechanical Engineering, University of Connecticut, 191 Auditorium Road, Unit 3139, Storrs, CT, 06269, USA. E-mail: wchiu@engr.uconn.edu; Tel: +860-486-3647*
[b]*Center for Innovative Fuel Cell and Battery Technologies, School of Materials Science and Engineering, Georgia Institute of Technology, Atlanta, Georgia, 30332, USA. E-mail: meilin.liu@mse.gatech.edu; Tel: +404-894-6114*
[c]*Advanced Photon Source, Argonne National Laboratory, Building 401, 9700 South Cass Avenue, Argonne, IL, 60439, USA. E-mail: yuwang@aps.anl.gov; Tel: +630-252-3789*
[d]*NSLS-II, Brookhaven National Laboratory, Upton, NY, 11973-5000, USA. E-mail: ychu@bnl.gov; Tel: +631-344-5582*

resolution[28] with phase specificity at up to one percent level sensitivity. Greater chemical sensitivity may be achieved by using scanning x-ray fluorescence tomography, albeit at a cost of substantially higher data acquisition times.[31–33] Three-dimensional elemental and microstructural data may also be obtained using focused ion beam-scanning electron microscopy (FIB-SEM), as has been demonstrated for SOFC and Li-ion battery electrodes.[34–36] Compared with SEM-based analytical techniques, x-ray techniques offer several key advantages. Multi-keV "hard" x-rays have a large penetration depth, on the order of tens to hundreds of microns for typical energy materials. Due to this large penetration depth, x-ray computed nanotomography can be used to obtain reliable 3D image data that represent the materials' full structure, including both surface and internal features at spatial resolution on the order of tens of nanometers, while maintaining sample integrity. In addition, full field elemental and chemical compositions can be mapped in 3D with the use of absorption contrast imaging and x-ray absorption near edge structure (XANES) spectroscopy, respectively. Finally, the absence of a charging effect, ability to operate at atmospheric conditions, and limited radiation damage mean that electrochemical devices can remain fully functional during imaging.[37,38] In this work, a synchrotron-based TXM has been used to perform XANES nanotomography for the identification and spatial mapping of materials potentially found in an SOFC exposed to sulfur poisoning. Measurements were performed at the Advanced Photon Source (APS) beamline 32-ID-C.[25,27] It has been demonstrated that this TXM configuration, using a similar zoneplate, can achieve a spatial resolution of 30 nm.[26]

As the initial step towards examining poisoned SOFC anodes, this study will focus on three-dimensional imaging and identification of controlled nickel (Ni) and nickel subsulfide (Ni_3S_2) samples. Ni_3S_2 was chosen for this study due to its possible formation as a poisoning phase during SOFC operational cycles. In previous work, Ni and nickel oxide (NiO) phases within controlled samples representative of an SOFC anode have been mapped and characterized by comparing tomographic scans above and below the Ni K-edge.[39] The case of mapping Ni and Ni_3S_2 phases that may occur within SOFC anodes presents a unique challenge compared to this previous work. Specifically, the spectral features that distinguish Ni and Ni_3S_2 are found between the Ni K-edge pre-edge region and the white line peak for each material, with considerably lower contrast.[40] The present work demonstrates the full field microstructural and chemical mapping capability of XANES nanotomography for such regions with large gradients in x-ray absorption.

In general, mapping light elements in low concentration (*e.g.* sulfur) in a 3D high-Z matrix (*e.g.* Ni/yttria-stabilizied zirconia, or Ni/YSZ) is fundamentally difficult with imaging techniques due to extremely minute x-ray absorption contrast from the light elements. Mapping sulfur composition in a Ni/YSZ matrix at the sulfur edge is not possible because of the low energy of the sulfur K-edge at 2.47 keV, which results in attenuation lengths of ~1 μm for dense Ni and YSZ. At this energy level, the sulfur signal (whether it be absorption as in this experiment or fluorescence emission in a fluorescence experiment) cannot escape the porous Ni/YSZ matrix without excessive attenuation unless the sample is sectioned down to a few microns in thickness. Below the Ni K-edge (8.33 keV), the attenuation lengths of Ni and YSZ are significantly higher, 20–25 μm, and, while attenuation of the signal by the Ni phase occurs above the K-edge, a sufficient signal is maintained, permitting discernment of the Ni and YSZ phases. Consequently the sulfur composition can only be measured indirectly *via* Ni by its XANES spectra. The absorption characteristics of Ni and Ni_3S_2 are not particularly distinguishable when comparing the two materials far below or above the Ni K-edge.[41,42] However, the Ni–S species do exhibit pre-edge structure attributed to electronic transition from 1s to 3d.[40] In this study, Ni speciation is identified using this pre-edge contrast.

Measurements were made with test samples fabricated from Ni foil and Ni_3S_2 powder. The Ni foil (99.95% pure, Alfa Aesar, Ward Hill, MA) was sectioned from a stock piece of foil approximately 2.54 μm thick. The Ni_3S_2 powder (99.7% pure, Sigma-Aldrich, St. Louis, MO) was produced from 150 mesh powder which was ground to produce a finer powder. Before examining the two species together, each was analyzed separately to calibrate the system by obtaining their detailed absorption spectra at 1 eV energy resolution. The Ni test sample was prepared by mounting a strip of Ni foil with several micron width on the tip of a pin. The TXM was used to obtain images of the sample at energy levels between 8325 eV and 8354 eV, at 1 eV increments and with an exposure time of three seconds. The absorption spectrum of pure Ni metal was obtained by examining the image intensity of the Ni foil at each energy relative to the surrounding blank area. The Ni_3S_2 sample was prepared by depositing powder on a copper transmission electron microscope grid. Its absorption spectrum was obtained in the same manner as pure Ni. Spectra from the two species were normalized by their pre- and post-edge linear absorption level and overlaid for comparison in Fig. 1.

A composite sample consisting of both Ni species was produced by depositing the Ni_3S_2 powder on Ni foil and allowing powder to cling to the metal. Projection images taken at several energy levels are shown in Fig. 1 to demonstrate the relative contrast change that is observed across the range of the spectra. To spatially resolve the two materials in 3D requires performing x-ray nanotomography at two or more energies chosen to maximize the relative contrast between the two species. Several such energies are denoted in Fig. 1, and for this study 8334 eV and 8341 eV were selected because Ni and Ni_3S_2 exhibit sufficiently significant absorption difference to lead to contrast reversal. X-ray nanotomography was performed on the composite sample at both of these energies by taking exposures with the sample rotated between −90° and +90° at 1° increments, with an exposure time of 3 s.

Each projection of the tomographic data sets at the two energy levels were aligned pixel-wise, and used to isolate the Ni and Ni_3S_2 based on the species' spectra in Fig. 1. The use of this species isolation technique has been described previously in detail for a system of Ni and NiO.[39] The resulting tomographic sets corresponding to the Ni and Ni_3S_2 species were reconstructed independently using an iterative algebraic reconstruction technique[43] and overlaid in 3D to illustrate the spatial distribution of the two species, as shown in the inset of Fig. 2. A ray tracing algorithm[44] was used to determine the phase size distribution (PSD) of each species, and the results are shown in Fig. 2. The Ni shows a clear peak at about 2.5 μm, as expected due to the foil thickness. It also shows tails on each side of the distribution, which is indicative of the fact that the region of interest is the tip of the foil, and therefore rays will have a wider distribution of lengths than if a simple cross section of the foil was considered. The Ni_3S_2 powder consists primarily of particles 4 μm in diameter or smaller, as expected due to the grinding process that was performed on the powder prior to use.

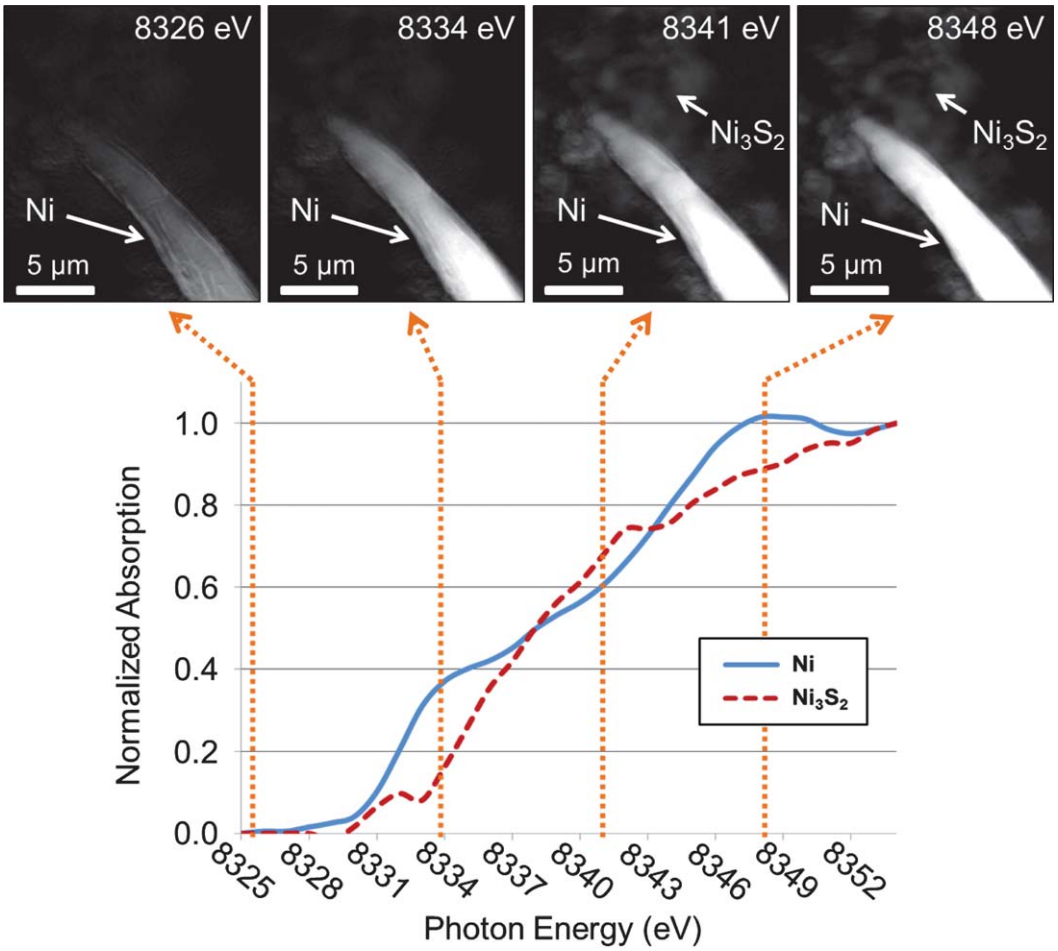

Fig. 1 Ni and Ni_3S_2 x-ray absorption spectra in the immediate vicinity of the Ni K-edge. The dotted lines show energy levels of interest in the XANES study. The absorption-mode projection images show the contrast change that can be seen in the two materials across the range of the spectra. Bright regions correspond to high absorption, while dark regions correspond to little or no absorption. In some regions, material is difficult to see due to its very low absorption.

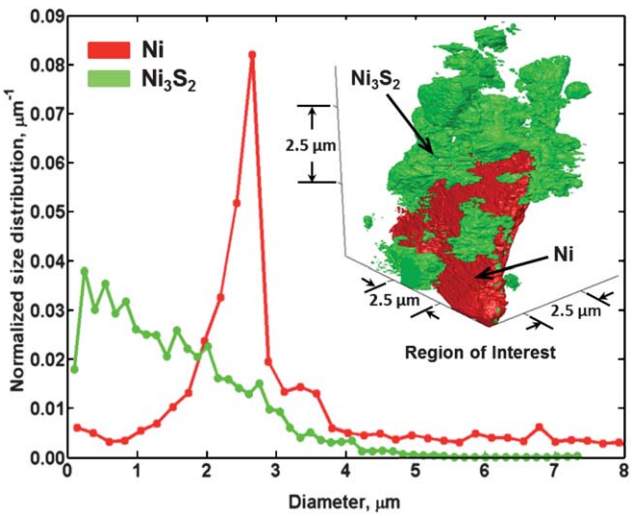

Fig. 2 Phase size distributions of Ni foil and Ni_3S_2 powder. The reconstructed region of interest is shown in the inset, with the Ni foil colored red and the Ni_3S_2 powder colored green.

Conclusions

Nanostructures of Ni and Ni_3S_2 were mapped in 3D using x-ray nanotomography combined with full field XANES spectroscopy. Distinct differences in the two species' absorption spectra in the immediate vicinity of the Ni K-edge were used to distinguish the materials. Reconstruction of the data provided a 3D volumetric data set of the phases, and allowed for calculation of the phase size distributions. PSD's were observed to be reasonable for the materials used. This work serves as a demonstration of a 3D analytical imaging approach for studying nano-scale and mesoscale chemical and electrochemical systems with elemental and chemical sensitivity. Considering the SOFC as an example, the ability to distinguish solid sulfur-containing phases from surrounding catalytic material has significant application in the understanding of the evolution of the electrode microstructure. The resolution and *in situ* imaging potential, particularly for energy materials, provide a valuable complementary analytical imaging toolset to light microscopy and electron microscopy techniques. Detailed observation of sulfur poisoning, on the nanoscale, may allow for a more complete understanding of the mechanisms by directly monitoring the process, and the locations within the system's microstructure that would be most susceptible to

its detrimental effects. The results presented are applicable to the examination of detailed nano-scale structures in numerous energy devices, including batteries, solar cells, fuel cells, and biomass fuel processing and reforming.

Acknowledgements

Financial support from an Energy Frontier Research Center on Science Based Nano-Structure Design and Synthesis of Heterogeneous Functional Materials for Energy Systems (HeteroFoaM Center) funded by the U.S. Department of Energy, Office of Science, Office of Basic Energy Sciences (Award DE-SC0001061) and the National Science Foundation (Award CBET-1134052) are gratefully acknowledged. Portions of this research were carried out at the Advanced Photon Source supported by the U.S. Department of Energy, Office of Science, Office of Basic Energy Sciences, under contract No. DE-AC02-06CH11357, and by the Brookhaven Science Associates, LLC under Contract No. DE-AC02-98CH10886.

Notes and references

1 Q. Wang, R. Gao and J. Li, *Appl. Phys. Lett.*, 2007, **90**, 143107, DOI: 10.1063/1.2716308.
2 J. Wang, S. Chou, S. Chew, J. Sun, M. Forsyth, D. R. MacFarlane and H. Liu, *Solid State Ionics*, 2008, **179**, 2379–2382, DOI: 10.1016/j.ssi.2008.09.007.
3 J. Wang and M. Liu, *J. Power Sources*, 2008, **176**, 23–30, DOI: 10.1016/j.jpowsour.2007.10.025.
4 K. W. Bae, H. S. Kim, G. B. Cho, K. W. Kim, K. K. Cho, J. H. Lee and T. H. Nam, *J. Power Sources*, 2009, **189**, 378–384, DOI: 10.1016/j.jpowsour.2008.08.012.
5 J. Kim, G. Cho, K. Kim, J. Ahn, G. Wang and H. Ahn, *Curr. Appl. Phys.*, 2011, **11**, S215–S218, DOI: 10.1016/j.cap.2010.11.082.
6 J. Kim, H. Ahn, H. Ryu, D. Kim, G. Cho, K. Kim, T. Nam and J. H. Ahn, *J. Power Sources*, 2008, **178**, 852–856, DOI: 10.1016/j.jpowsour.2007.09.067.
7 H. Sun, D. Qin, S. Huang, X. Guo, D. Li, Y. Luo and Q. Meng, *Energy Environ. Sci.*, 2011, **4**, 2630–2637, DOI: 10.1039/c0ee00791a.
8 A. Braun, M. Janousch, J. Sfeir, J. Kiviaho, M. Noponen, F. E. Huggins, M. J. Smith, R. Steinberger-Wilckens, P. Holtappels and T. Graule, *J. Power Sources*, 2008, **183**, 564–570, DOI: 10.1016/j.jpowsour.2008.05.048.
9 A. J. Allen, J. Ilavsky and A. Braun, *Adv. Eng. Mater.*, 2009, **11**, 495–501, DOI: 10.1002/adem.200800357.
10 Zhe Cheng, J. H. Wang, Y. M. Choi, L. Yang, M. C. Lin and M. Liu, *Energy Environ. Sci.*, 2011, **4**, 4380–4409, DOI: 10.1039/c1ee01758f.
11 K. Haga, S. Adachi, Y. Shiratori, K. Itoh and K. Sasaki, *Solid State Ionics*, 2008, **179**, 1427–1431, DOI: 10.1016/j.ssi.2008.02.062.
12 F. N. Cayan, M. Zhi, S. R. Pakalapati, I. Celik, N. Wu and R. Gemmen, *J. Power Sources*, 2008, **185**, 595–602, DOI: 10.1016/j.jpowsour.2008.06.058.
13 K. Sato and K. Fujimoto, *Catal. Commun.*, 2007, **8**, 1697–1701, DOI: 10.1016/j.catcom.2007.01.028.
14 L. Li, C. Howard, D. L. King, M. Gerber, R. Dagle and D. Stevens, *Ind. Eng. Chem. Res.*, 2010, **49**, 10144–10148, DOI: 10.1021/ie101032x.
15 S. Matsumoto, Y. Ikeda, H. Suzuki, M. Ogai and N. Miyoshi, *Appl. Catal., B*, 2000, **25**, 115–124.
16 G. Di Carlo, G. Melaet, N. Kruse, L. F. Liotta, G. Pantaleo and A. M. Venezia, *Chem. Commun.*, 2010, **46**, 6317–6319.
17 G. Corro, C. Cano and J. L. G. Fierro, *J. Mol. Catal. A: Chem.*, 2010, **315**, 35–42, DOI: 10.1016/j.molcata.2009.08.023.
18 Y. Chen, C. Xie, Y. Li, C. Song and T. B. Bolin, *Phys. Chem. Chem. Phys.*, 2010, **12**, 5707–5711.
19 C. Xie, Y. Chen, Y. Li, X. Wang and C. Song, *Appl. Catal., A*, 2010, **390**, 210–218, DOI: 10.1016/j.apcata.2010.10.012.
20 Z. Cheng, S. Zha and M. Liu, *J. Electrochem. Soc.*, 2006, **153**, A1302–A1309.
21 M. Gong, X. Liu, J. Trembly and C. Johnson, *J. Power Sources*, 2007, **168**, 289–298, DOI: 10.1016/j.jpowsour.2007.03.026.
22 L. Yang, S. Wang, K. Blinn, M. Liu, Z. Liu, Z. Cheng and M. Liu, *Science*, 2009, **326**, 126–129.
23 Y. Huang, R. I. Dass, Z. King and J. B. Goodenough, *Science*, 2006, **312**, 254–257.
24 N. Lakshminarayanan and U. S. Ozkan, *Appl. Catal., A*, 2011, **393**, 138–145, DOI: 10.1016/j.apcata.2010.11.034.
25 K. N. Grew, Y. S. Chu, J. Yi, A. A. Peracchio, J. R. Izzo Jr., Y. Hwu, F. De Carlo and W. K. S. Chiu, *J. Electrochem. Soc.*, 2010, **157**, B783–B792.
26 Y. T. Chen, T. N. Lo, Y. S. Chu, J. Yi, C. J. Liu, J. Y. Wang, C. L. Wang, C. W. Chiu, T. E. Hua, Y. Hwu, Q. Shen, G. C. Yin, K. S. Liang, H. M. Lin, J. H. Je and G. Margaritondo, *Nanotechnology*, 2008, **19**, 395302, DOI: 10.1088/0957-4484/19/39/395302.
27 Y. S. Chu, J. M. Yi, F. De Carlo, Q. Shen, W. K. Lee, H. J. Wu, C. L. Wang, J. Y. Wang, C. J. Liu, C. H. Wang, S. R. Wu, C. C. Chien, Y. Hwu, A. Tkachuk, W. Yun, M. Feser, K. S. Liang, C. S. Yang, J. H. Je and G. Margaritondo, *Appl. Phys. Lett.*, 2008, **92**, 103119, DOI: 10.1063/1.2857476.
28 T. Y. Chen, Y. T. Chen, C. L. Wang, I. M. Kempson, W. K. Lee, Y. S. Chu, Y. Hwu and G. Margaritondo, *Opt. Express*, 2011, **19**, 19919–19924, DOI: 10.1364/OE.19.019919.
29 P. R. Shearing, D. J. L. Brett and N. P. Brandon, *Int. Mater. Rev.*, 2010, **55**, 347–363, DOI: 10.1179/095066010X12777205875679.
30 J. Laurencin, R. Quey, G. Delette, H. Suhonen, P. Cloetens and P. Bleuet, *J. Power Sources*, 2012, **198**, 182–189, DOI: 10.1016/j.jpowsour.2011.09.105.
31 P. Bleuet, P. Cloetens, P. Gergaud, D. Mariolle, N. Chevalier, R. Tucoulou, J. Susini and A. Chabli, *Rev. Sci. Instrum.*, 2009, **80**, 056101, DOI: 10.1063/1.3117489.
32 P. Bleuet, P. Gergaud, L. Lemelle, P. Bleuet, R. Tucoulou, P. Cloetens, J. Susini, G. Delette and A. Simionovici, *TrAC, Trends Anal. Chem.*, 2010, **29**, 518–527, DOI: 10.1016/j.trac.2010.02.011.
33 M. D. De Jonge and S. Vogt, *Curr. Opin. Struct. Biol.*, 2010, **20**, 606–614, DOI: 10.1016/j.sbi.2010.09.002.
34 J. R. Wilson, W. Kobsiriphat, R. Mendoza, H. Y. Chen, J. M. Hiller, D. J. Miller, K. Thornton, P. W. Voorhees, S. B. Adler and S. A. Barnett, *Nat. Mater.*, 2006, **5**, 541–544.
35 J. R. Wilson, A. T. Duong, M. Gameiro, H. Y. Chen, K. Thornton, D. R. Mumm and S. A. Barnett, *Electrochem. Commun.*, 2009, **11**, 1052–1056, DOI: 10.1016/j.elecom.2009.03.010.
36 J. R. Wilson, J. S. Cronin, S. A. Barnett and S. J. Harris, *J. Power Sources*, 2011, **196**, 3443–3447, DOI: 10.1016/j.jpowsour.2010.04.066.
37 A. Haibel, I. Manke, A. Melzer and J. Banhart, *J. Electrochem. Soc.*, 2010, **157**, A387–A391, DOI: 10.1149/1.3294566.
38 S. C. Chao, Y. C. Yen, Y. F. Song, Y. M. Chen, H. C. Wu and N. L. Wu, *Electrochem. Commun.*, 2010, **12**, 234–237, DOI: 10.1016/j.elecom.2009.12.002.
39 G. J. Nelson, W. M. Harris, J. R. Izzo Jr., K. N. Grew, W. K. S. Chiu, Y. S. Chu, J. Yi, J. C. Andrews, Y. Liu and P. Pianetta, *Appl. Phys. Lett.*, 2011, **98**, 173109, DOI: 10.1063/1.3574774.
40 W. Niemann, B. S. Clausen and H. Topsøe, *Catal. Lett.*, 1990, **4**, 355–363.
41 B. L. Henke, E. M. Gullikson and J. C. Davis, X-ray interactions: photoabsorption, scattering, transmission, and reflection at E = 50–30000 eV, Z = 1–92, 1993.
42 F. E. Huggins, N. Shah, G. P. Huffman and J. D. Robertson, *Fuel Process. Technol.*, 2000, **65–66**, 203–218.
43 Y. J. Liu, P. P. Zhu, B. Chen, J. Y. Wang, Q. X. Yuan, W. X. Huang, H. Shu, E. R. Li, X. S. Liu, K. Zhang, H. Ming and Z. Y. Wu, *Phys. Med. Biol.*, 2007, **52**, L5–L13, DOI: 10.1088/0031-9155/52/12/L01.
44 K. N. Grew, A. A. Peracchio and W. K. S. Chiu, *J. Power Sources*, 2010, **195**, 7943–7958, DOI: 10.1016/j.jpowsour.2010.07.006.

